

# Catalysis Science & Technology

Accepted Manuscript



This is an *Accepted Manuscript*, which has been through the Royal Society of Chemistry peer review process and has been accepted for publication.

*Accepted Manuscripts* are published online shortly after acceptance, before technical editing, formatting and proof reading. Using this free service, authors can make their results available to the community, in citable form, before we publish the edited article. We will replace this *Accepted Manuscript* with the edited and formatted *Advance Article* as soon as it is available.

You can find more information about *Accepted Manuscripts* in the [Information for Authors](#).

Please note that technical editing may introduce minor changes to the text and/or graphics, which may alter content. The journal's standard [Terms & Conditions](#) and the [Ethical guidelines](#) still apply. In no event shall the Royal Society of Chemistry be held responsible for any errors or omissions in this *Accepted Manuscript* or any consequences arising from the use of any information it contains.

# Verification of dual cycle mechanism for methanol-to-olefins conversion in HSAPO-34: Methylbenzenes-based cycle from DFT calculations

Chuan-Ming Wang,\* Yang-Dong Wang, Zai-Ku Xie\*

Shanghai Research Institute of Petrochemical Technology, SINOPEC, Shanghai 201208, China

\*Tel. : (+86)21-68462197; Fax: (+86)21-68462283

E-Mail: [wangcm.sshy@sinopec.com](mailto:wangcm.sshy@sinopec.com), and [xzk@sinopec.com](mailto:xzk@sinopec.com)

## Abstract

Understanding the reaction mechanism of methanol-to-olefins (MTO) conversion is a challenging issue in zeolite catalysis. Using BEEF-vdW functional with van der Waals (vdW) correlation, we systematically investigated methylbenzenes(MBs)-based side chain hydrocarbon pool (HP) mechanism in HSAPO-34 zeotype catalyst. The inclusion of vdW correction is very important, especially in stabilizing the intermediates and transition states with delocalized ion pair structures. The rate-determining step is identified as the propagation of side alkyl chains via the methylation of exocyclic double bond. No obvious difference was observed in catalytic activity between different hydrocarbon pool species (hexamethylbenzene, tetramethylbenzene, and p-xylene). Ethene appears to be more favorable than propene as the product. These theoretical results strongly support the dual cycle mechanism in which MBs-based and olefins-based routes run simultaneously during the MTO conversion, and ethene is produced through MBs-based route.

## 1. Introduction

The methanol-to-olefins (MTO) conversion has attracted much attention in academic and industrial communities because it is one of the most important technologies to produce bulk chemicals from non-oil resources like coal, natural gas, or biomass.<sup>1,2</sup> This process is usually catalyzed by acid zeolite or zeotype materials. HSAPO-34 and HZSM-5 have proven to be the most promising catalysts for the MTO conversion.<sup>3</sup> However, the product distribution differs too much on both catalysts.<sup>4</sup> The selectivity to ethene and propene is over 80% in HSAPO-34, while higher olefins like butenes appear in relatively large amount in HZSM-5. This difference in selectivity and the complicated distribution of products (olefins, alkanes, aromatics) make it very difficult to understand this process and to control catalytic activity and selectivity.<sup>5-12</sup>

Understanding the reaction mechanism is one of challenging topics in MTO conversion.<sup>13-17</sup> It is generally accepted that the MTO conversion proceeds through hydrocarbon pool (HP) mechanism. In this mechanism, certain organic species, known as hydrocarbon pool species, are involved in the reaction. It was experimentally and theoretically proved that methylbenzenes (MBs) or/and olefins encapsulated in zeolites are the predominant HP species.<sup>18,19</sup> A dual cycle concept in which MBs-based and olefins-based routes run simultaneously was then proposed from isotope labeling experimental results.<sup>20-22</sup> Svelle et al. found that the <sup>13</sup>C contents in the propene to hexene are very similar with the time evolution, while the isotopic composition is much less in ethene and aromatics. Previously, we have theoretically investigated olefins-based cycle, and constructed a reaction network to rationalize the formation of olefins, alkanes, and aromatics.<sup>23</sup> The distribution of cracking precursors is proposed to affect the selectivity. However, the MBs-based cycle still remains ambiguous. Two different reaction pathways, side chain and

paring, were once proposed for the evolution of MBs-based HP species.<sup>16</sup>

In the side chain route, ethene or propene is produced through the elimination of side alkyl chains, and which are formed via the methylation step.<sup>24</sup> A lot of theoretical work in cluster or periodic zeolite or zeotype models have been conducted to address this side chain route. Using simple cluster model, Arstad et al. first studied the thermodynamics of the side chain pathway.<sup>25</sup> The zeolite topology effect on methylation step was further investigated by Lesthaeghe et al. using QM/MM model.<sup>26</sup> We also addressed the effect of HP species on catalytic activity and selectivity using periodic HSAPO-34 model.<sup>27</sup> However, The elimination of side ethyl chain is very energy demanding. More recently, De Wispelaere et al. proposed a complete low barrier side chain route in extended finite cluster HSAPO-34.<sup>28</sup>

In the paring route, the side alkyl chains are formed by the contraction of six-membered rings to five-membered rings.<sup>29</sup> Our previous theoretical results indicated that paring route plays minor role for the MTO conversion in HSAPO-34.<sup>29</sup> However, the scrambling phenomena of ring carbon into olefins indicates that paring route may be operative from experimental point of view.<sup>30, 31</sup> Based on isotope labeling experiments, it was found that one carbon atom in most ethene and propene is from the ring carbon in MBs.

Despite great progress made experimentally and theoretically, the MTO reaction mechanism is still a hot area of dispute.<sup>29-44</sup> For example, the characteristics of HP species and its effect on catalytic properties are unclear. The preference of the side chain or paring pathways in the MBs-based HP mechanism is unsettled. In this work, employing newly developed BEEF-vdW functional including van der Waals (vdW) correlation,<sup>45</sup> we systematically investigate MBs-based side chain HP mechanism.

Hexamethylbenzene (HMB), 1,2,3,5-tetramethylbenzene (TMB), and p-xylene (PX) were selected as represented HP species in HSAPO-34. We attempt to understand the following questions: 1) What's the rate-determining steps? 2) How do HP structures influence catalytic activity and selectivity?

## 2. Computational methods and modeling

All density functional theory (DFT) calculations were carried out using GPAW package, a real-space grid implementation of the projector augmented-wave method.<sup>46, 47</sup> The grid spacing in real-space is 0.20 Å. The sampling of Brillouin zone is only with  $\Gamma$  point.<sup>48</sup> The Bayesian error estimation functional with van der Waals correlation (BEEF-vdW) was employed.<sup>45, 49</sup> The climbing image nudged elastic band (CI-NEB) method was used to locate all the transition states.<sup>50</sup> A force threshold of 0.03 eV/Å was used for the geometry optimization of intermediates and transition states.

The HSAPO-34 is represented by 36T hexagonal cell having one acid site at O2 position, as showed in Fig. 1. The optimized lattice constants are  $a = b = 13.80$  Å,  $c = 15.04$  Å, which is similar to the experimental results [ $a = b = 13.73$  Å,  $c = 15.05$  Å].<sup>51</sup> The interaction between organic species and their images can completely be avoided using this periodic 36T model (see Fig. 1). All atoms in the cell were allowed to relax in the calculations with the lattice constants being fixed.

### 3. Results and Discussion

The MBs-based side chain HP mechanism is shown in Scheme 1. The entire process encompasses side chain growth through methylation step, and side chain elimination step. However, the elimination of side chain into olefins, especially, ethene, is highly energy-demanding through the direct step or indirect step via intermediates with sipro structure.<sup>24, 27</sup> More recently, the elimination step was addressed by De Wispelaere et al. who proposed one more feasible route to lower the elimination barriers.<sup>28</sup> In this route (M4/M6  $\rightarrow$  M10), the methyl group firstly shifts along the ring to the carbon atom bonding to the side ethyl/isopropyl chain. Then, the side chain splits off from the carbon ring to produce ethene or propene, and to recover the HP structure. In the following, based on the periodic DFT calculations with vdW correction, we elucidate the reaction thermodynamics and kinetics of HMB, TMB, and PX-based HP pathways, and then address the effect of HP structures on the MTO catalytic activity and selectivity. The optimized geometries of transition states are listed in the supplementary information.

#### 3.1 HMB-based side chain HP pathway

Fig. 2 is the energy diagram of the HMB-based side chain HP pathway in HSAPO-34 simulated using periodic 36T model. The energy barriers for each step are summarized in Table 1. Besides the results calculated using BEEF-vdW functional, the single point results are also calculated utilizing two other functionals with vdW correction (vdW-DF, and vdW-DF2), and PBE functional.<sup>52-54</sup>

The propagation of side alkyl chains was first elucidated. The adsorption energy of methanol is calculated to be around 0.90 eV, similar to previous calculated results.<sup>24</sup> The first methylation step, forming heptamethylbenzenium ion (heptaMB<sup>+</sup>, M1  $\rightarrow$  M2), need to overcome an energy barrier of about 1.09 eV, similar to that

calculated in periodic 12T model (1.10 eV) corrected by PBE-D method, but higher than the calculated results in 44T cluster model (0.80 eV).<sup>27, 28</sup> At the transition state TS1-2, the distances of the breaking O-C bond and the forming C-C bond are 2.11 and 2.28 Å, respectively (see Fig. 3). The next step is the deprotonation of heptaMB<sup>+</sup> ion to form the intermediate with exocyclic double bond (M3). Before the deprotonation is the rotation of heptaMB<sup>+</sup> to make the para-methyl group close to the acid site (M2-R). The calculated barrier (1.02 eV) of the deprotonation is higher than that calculated using PBE and in other models (0.52 ~ 0.79 eV). This exocyclic double bond is the initial structure for the propagation of side alkyl chains. The side ethyl group is formed through the second methylation step (TS3-4). The energy barrier is calculated to be 0.97 eV. The distances of the breaking O-C bond and the forming C-C bond are 1.94 and 2.38 Å, respectively (see Fig. 3). Through the subsequent deprotonation step (TS4-5) and the third methylation step (TS5-6), side isopropyl group can be formed as well. We can see that the energy barrier for the second deprotonation step (1.37 eV) is much higher than the first deprotonation step (1.02 eV). However, the barrier for the third methylation step (0.95 eV) is similar to the second step.

From intermediates with side ethyl (M4) or isopropyl (M6) groups, several routes were proposed to eliminate side alkyl chains into ethene or propene. We once proposed an indirect pathway assisted by water in which intermediates with spiro structure were formed.<sup>24</sup> However, the elimination barrier to ethene is very high. More recently, De Wispelaere et al. proposed a low barrier pathway for the elimination steps.<sup>28</sup> As indicated in Scheme 1, they pointed out that the gem-methyl group first shift along the carbon ring to the carbon atom bonding to the side alkyl groups. As the bonding of the side chains to the ring is weakened, the final elimination step energetically becomes more possible.

As can be seen from Table 1, the methyl shift barriers in the first (TS-MS1) and second (TS-MS2) steps are found to be insensitive to the vdW correction and model. In the ethene elimination route, both barriers are in the range of 0.76 ~ 0.84 eV for the first step, and 0.88 ~ 0.96 eV for the second step. In the propene elimination route, those are respectively in the range of 0.83 ~ 0.91 eV, and 0.91 ~ 1.12 eV.

However, for the third methyl shift step (TS-MS3), the energy barrier calculated in periodic 36T model are much lower than those calculated in 44T cluster model (0.40 vs. 0.70 eV in ethene formation route, and 0.53 vs. 0.90 eV in propene formation route).<sup>28</sup> As for the final elimination step, a concerted mechanism was proposed by De Wispelaere et al.<sup>28</sup> As shown in Fig. 3, at the transition state, the terminal methyl group in the side chain donates one proton to the framework mediated by water when the bonding to the carbon ring breaks. The energy barriers are calculated to be 1.12 eV and 0.66 eV for the elimination of ethyl and isopropyl groups, much higher than those calculated in 44T cluster model (0.63eV, and 0.35 eV). At both transition states, the distances of the breaking H-C and the forming H-O bonds are 1.32 ~ 1.36 Å, while the breaking C-C bond distances are 2.70 and 2.86 Å, similar to the geometry structures in 44T cluster model (2.62 and 2.81 Å).<sup>28</sup>

As can be seen from Fig. 2, the inclusion of vdW correction greatly stabilizes the benzenium ions featuring ion pair structure, like M2, M4, M6 ~ M10. M2 is stabilized by about 0.40 eV due to vdW correction. M4, and M6 to M10 are usually stabilized by over 0.60 eV. However it less influences the transition state energies in the deprotonation steps. TS2-3 and TS4-5 are only stabilized by 0.10 eV. Therefore, both energy barriers calculated using BEEF-vdW are much higher than those calculated with PBE. Due to the similar effect of vdW correction to the initial state and

transition state in the methylation and methyl shift steps, these energy barriers are relatively less affected by vdW correction.

### 3.2 TMB-based and PX-based side chain HP pathway

Fig. 4 shows the energy diagrams of TMB-based and PX-based side chain HP mechanism in HSAPO-34. The energy barriers for each elementary step are summarized in Table 2. The variation of methanol adsorption energy in HSAPO-34 is around 0.1 eV affected by MBs. Compared to M1, The intermediates in the early steps (M2, M3, and M4) are less stable than those in HMB-based pathway. For instance, the relative energies of M4 are around -0.70 ~ -0.90 eV in TMB, and PX-based pathways, while those are about -1.20 eV in HMB-based pathway. This is due to the extra methyl groups in the carbon ring. For the intermediates in the latter steps (M5 ~ M9), it can be seen that the benzenium ions with side isopropyl chain (M9 in TMB-based pathway, and M7 in PX-based pathway) are the most stable intermediates. The three methylated carbenium ions (M2, M4, and M6) become more and more stable with the side chain growth.

In TMB-based pathway, the energy barriers are 1.19, 0.90, and 0.99 eV for the first, the second, and the third methylation step, respectively. The energy barriers in the formation of the exocyclic double bond by deprotonation are calculated to be 0.61 and 0.86 eV mediated by water. In three steps of the methyl shift along the carbon ring, the barriers are calculated to be around 0.55, 0.85, and 0.25 eV, respectively, irrelevant to the side alkyl chains. The elimination of side ethyl and isopropyl groups needs to overcome energy barriers of about 1.12 and 0.66 eV, similar to those in HMB-based pathway. At the transition states of the final elimination step, the distances of the breaking H-C and forming H-O are in the range of 1.30 ~ 1.38 Å. The breaking C-C distances are 2.69 and 2.98 Å respectively for the

production of ethene and propene in TMB-based pathway.

We now move to the energy evolution in PX-based pathway. With the decrease of the number of methyl groups, the first methylation becomes more difficult. The energy barrier of this step is 1.31 eV, higher than that in HMB-based and TMB-based pathways. However, the second and third methylations need to overcome a similar barrier height (0.8 ~ 1.0 eV) as in other pathways. The two deprotonation steps to form exocyclic double bond are slightly facile (0.52, and 0.72 eV). In the methyl group shift steps, the energy barriers are calculated to be among the range of 0.49 ~ 0.71 eV in the elimination route of ethyl group, and 0.71 ~ 0.78 eV in the elimination route of isopropyl group. The final elimination steps are much easier than other two pathways. The energy barriers are only 0.71, and 0.22 eV, respectively to produce ethene and propene. The breaking H-C distances are 1.28, and 1.26 Å, and the forming H-O distances are 1.41, and 1.46 Å in the transition states of final elimination step of side ethyl and isopropyl groups.

### 3.3 General Discussion

As can be seen from Table 1 and Table 2, the energy barriers in three methylation steps (TS1-2, TS3-4, and TS5-6), three methyl group shift steps (TS-MS1, TS-MS2, and TS-MS3) are less sensitive to the vdW correction in HMB, TMB, and PX-based pathways. The energy barriers usually differ less than 0.20 eV for each elementary step using different functionals (BEEF-vdW, vdW-DF, vdW-DF2, and PBE). This is because both the initial state and transition state show a similar distribution of positive charge in this kind of elementary steps. However, the vdW correction greatly affects the barriers in the deprotonation steps (TS2-3, and TS4-5) to form exocyclic double bond. The vdW correction energies are around 0.40 eV for the deprotonation steps. This can be explained as follows. The vdW correction

greatly stabilizes ion pair structures (M2, and M4) that positive charge delocalized in carbenium ions. The deprotonation transition state, however, adopted a late transition state structure in which positive charge localized in  $\text{H}_3\text{O}^+$  motif, and which is less sensitive to vdW correction. A similar reason that the positive charge becomes more localized into  $\text{H}_3\text{O}^+$  motif from initial state to transition state could explain the effect of vdW correction to the final elimination step of side ethyl and isopropyl groups. The correction energies are around 0.20 eV in TS9-10 for ethene and propene formation in three different pathways. So the energy barriers of the elementary steps that experience obvious change of positive charge distribution in zeolite catalysis is sensitive to vdW correlation.

We are currently in the position to understand the relationship between the structures of MBs and the catalytic activity and selectivity. For clarity, we divide the entire pathway into two parts: side alkyl chain propagation, and ethene/propene production through methyl group shift and elimination steps. Table 3 summarized the over energy barriers for both parts. For the production of ethene, it is identified that the side chain growth through the second methylation is the rate-determining step because the energy barriers in the methyl group shift and elimination are lower than that of side chain propagation in all three MBs. For the production of propene, the rate-determining step is the third methylation in HMB-based pathway, and the second in the other pathways. Therefore, side chain propagation is confirmed to be the rate-determining step in MBs-based side chain HP mechanism. By comparing the energy barriers to produce ethene and propene (1.26 vs. 1.77 eV in HMB, 1.12 vs. 1.28 eV in TMB, 0.79 vs. 1.02 eV in PX), we can find that ethene is more selective than propene as the product in this reaction pathway. The overall energy barriers for the catalytic cycle are 1.48, 1.60, and 1.58 eV for HMB, TMB, and PX-based pathway. As the change is only 0.12 eV, and which lies within the typical DFT error range (ca.

0.20 eV), we conclude that no noticeable difference in catalytic activity between HMB, TMB, and PX, similar to our previous findings that HMB is not more active than MBs with less methyl groups.<sup>27</sup>

Previously, we once concluded that olefins are likely to be the dominating hydrocarbon pool species in HSAPO-34 because of the relative lower energy barriers in olefins-based cycle compared to MBs-based cycle when calculated using PBE functional.<sup>23</sup> The overall energy barriers are calculated to be over 1.80 eV using PBE functional in periodic 12T HSAPO-34, similar to the PBE results in this work (over 1.70 eV).<sup>24, 27</sup> However, the inclusion of vdW correction decreasing the overall energy barriers by about 0.20 eV, and the identification of an energetically more feasible elimination pathway of side ethyl group, make MBs-based cycle more competitive than before. The importance of MBs-based cycle in HSAPO-34 was recently highlighted by Li et al. because they found that the selectivity to ethene is above thermodynamic equilibrium.<sup>55</sup> A dual cycle concept firstly introduced by Svelle et al. is therefore strongly supported.<sup>20-22</sup> In the dual cycle mechanism (see Scheme 2), Svelle et al. proposed that ethene is produced exclusively from MBs-based cycle, while propene and higher olefins are formed from olefins-based cycle. The interplay between both cycles as a result of catalyst structures and reaction conditions dedicates to the selectivity.<sup>30, 56</sup> Westgård et al. observed that the olefins-based cycle is promoted in lower acid strength zeolite.<sup>30</sup> Propene to pentenes are found to be the predominant products in HSAPO-5 produced via olefins-based cycle. The effect of acid strength on the role of two cycles may come from the different sensitivity of rate-determining steps to acid strength.

Understanding the detailed evolution of olefins-based cycle is of paramount importance as well. We once built a full olefins-based cycle in HSAPO-34, in which

olefins, aromatics, and alkanes are formulated within the reaction network.<sup>23</sup> A stepwise decrease in the cracking barriers was observed with the carbon atom number of cracking precursors. The cracking into propene or longer olefins (if they can diffuse from catalyst pores) is preferential than that into ethene except C<sub>5</sub><sup>+</sup> and C<sub>6</sub><sup>+</sup> ions, which however requires to overcome higher energy barriers. The easiness of olefin methylation to longer chains makes it very difficult to limit the length of cracking precursors, especially in zeolites with open framework structure, like HZSM-5, HSAPO-5. So this work confirms that ethene exclusively produced through the MBs-based cycle, and both MBs and olefins are hydrocarbon pool species depending on catalyst structures and reaction conditions. The dual cycle mechanism is therefore proved from theoretical point of view.

#### 4. Conclusions

In summary, the MBs-based side chain hydrocarbon pool mechanism was revisited using periodic DFT calculations with vdW correlation. The propagation of side alkyl chains through the methylation of exocyclic double bond is identified as the rate-determining step. It was found that the overall energy barriers for the MTO conversion decrease by about 0.20 eV with the inclusion of vdW correction compared to PBE results. No noticeable difference in overall energy barriers (1.48 ~ 1.60 eV) can be observed in HMB, TMB, and PX-based cycle. We also demonstrated that ethene is more selective than propene in MBs-based cycle. All these calculated results strongly support that the MTO conversion proceeds through the dual cycle mechanism. Subsequently, understanding the interplay between aromatics-based cycle and olefins-based cycle is therefore of paramount importance in the MTO conversion.

**Acknowledgements.** This work is supported by National Basic Research Program of

China (2009CB623504), National Science Foundation of China (21103231), and Shanghai Science Foundation (11ZR1449700).

Electronic Supplementary Information (ESI) available. See DOI: 10.1039/b000000x/

## References

1. M. Stocker, *Micropor. and Mesopor. Mater.*, 1999, **29**, 3-48.
2. F. J. Keil, *Micropor. and Mesopor. Mater.*, 1999, **29**, 49-66.
3. B. M. Lok, C. A. Messina, R. L. Patton, R. T. Gajek, T. R. Cannan and E. M. Flanigen, *J. Am. Chem. Soc.*, 1984, **106**, 6092-6093.
4. T. Yokoi, M. Yoshioka, H. Imai and T. Tatsumi, *Angew. Chem. Int. Ed.*, 2009, **121**, 9884-9887.
5. S. Teketel, W. Skistad, S. Benard, U. Olsbye, K. P. Lillerud, P. Beato and S. Svelle, *ACS Catal.*, 2012, **2**, 26-37.
6. C. M. Wang, B. W. Li, Y. D. Wang and Z. K. Xie, *J. Energy Chem.*, 2013, **22**, 914-918.
7. B. P. C. Hereijgers, F. Bleken, M. H. Nilsen, S. Svelle, K. P. Lillerud, M. Bjorgen, B. M. Weckhuysen and U. Olsbye, *J. Catal.*, 2009, **264**, 77-87.
8. S. Ilias and A. Bhan, *J. Catal.*, 2012, **290**, 186-192.
9. S. Teketel, U. Olsbye, K.-P. Lillerud, P. Beato and S. Svelle, *Micropor. and Mesopor. Mater.*, 2010, **136**, 33-41.
10. F. L. Bleken, T. V. W. Janssens, S. Svelle and U. Olsbye, *Micropor. and Mesopor. Mater.*, 2012, **164**, 190-198.
11. W. Dai, X. Wang, G. Wu, N. Guan, M. Hunger and L. Li, *ACS Catal.*, 2011, **1**, 292-299.
12. D. Mores, E. Stavitski, M. H. F. Kox, J. Kornatowski, U. Olsbye and B. M. Weckhuysen, *Chem. Eur. J.*, 2008, **14**, 11320-11327.
13. U. Olsbye, S. Svelle, M. Bjorgen, P. Beato, T. V. W. Janssens, F. Joensen, S. Bordiga and K. P. Lillerud, *Angew. Chem. Int. Ed.*, 2012, **51**, 5810-5831.
14. K. Hemelsoet, J. Van der Mynsbrugge, K. De Wispelaere, M. Waroquier and V. Van Speybroeck, *ChemPhysChem*, 2013, **14**, 1526-1545.
15. J. F. Haw, W. G. Song, D. M. Marcus and J. B. Nicholas, *Acc. Chem. Res.*, 2003, **36**, 317-326.
16. U. Olsbye, M. Bjorgen, S. Svelle, K. P. Lillerud and S. Kolboe, *Catal. Today*, 2005, **106**, 108-111.
17. S. Ilias and A. Bhan, *ACS Catal.*, 2012, **3**, 18-31.
18. W. G. Song, J. F. Haw, J. B. Nicholas and C. S. Heneghan, *J. Am. Chem. Soc.*, 2000, **122**, 10726-10727.
19. B. Arstad and S. Kolboe, *J. Am. Chem. Soc.*, 2001, **123**, 8137-8138.
20. S. Svelle, F. Joensen, J. Nerlov, U. Olsbye, K. P. Lillerud, S. Kolboe and M. Bjorgen, *J. Am. Chem. Soc.*, 2006, **128**, 14770-14771.
21. M. Bjorgen, S. Svelle, F. Joensen, J. Nerlov, S. Kolboe, F. Bonino, L. Palumbo, S. Bordiga and U. Olsbye, *J. Catal.*, 2007, **249**, 195-207.
22. S. Svelle, U. Olsbye, F. Joensen and M. Bjorgen, *J. Phys. Chem. C*, 2007, **111**, 17981-17984.
23. C. M. Wang, Y. D. Wang and Z. K. Xie, *J. Catal.*, 2013, **301**, 8-19.

24. C. M. Wang, Y. D. Wang, Z. K. Xie and Z. P. Liu, *J. Phys. Chem. C*, 2009, **113**, 4584-4591.
25. B. Arstad, J. B. Nicholas and J. F. Haw, *J. Am. Chem. Soc.*, 2004, **126**, 2991-3001.
26. D. Lesthaeghe, B. De Sterck, V. Van Speybroeck, G. B. Marin and M. Waroquier, *Angew. Chem. Int. Ed.*, 2007, **46**, 1311-1314.
27. C. M. Wang, Y. D. Wang, H. X. Liu, Z. K. Xie and Z. P. Liu, *J. Catal.*, 2010, **271**, 386-391.
28. K. De Wispelaere, K. Hemelsoet, M. Waroquier and V. Van Speybroeck, *J. Catal.*, 2013, **305**, 76-80.
29. C. M. Wang, Y. D. Wang, H. X. Liu, Z. K. Xie and Z. P. Liu, *Micropor. and Mesopor. Mater.*, 2012, **158**, 264-271.
30. M. Westgård Erichsen, S. Svelle and U. Olsbye, *J. Catal.*, 2013, **298**, 94-101.
31. S. Ilias and A. Bhan, *J. Catal.*, 2014, **311**, 6-16.
32. D. S. Wragg, M. G. O. Brien, F. L. Bleken, M. Di Michiel, U. Olsbye and H. Fjellvag, *Angew. Chem. Int. Ed.*, 2012, **51**, 7956-7959.
33. D. S. Wragg, D. Akporiaye and H. Fjellvag, *J. Catal.*, 2011, **279**, 397-402.
34. Z. M. Cui, Q. Liu, W. G. Song and L. J. Wan, *Angew. Chem. Int. Ed.*, 2006, **45**, 6512-6515.
35. L. Palumbo, F. Bonino, P. Beato, M. Bjorgen, A. Zecchina and S. Bordiga, *J. Phys. Chem. C*, 2008, **112**, 9710-9716.
36. D. M. Marcus, K. A. McLachlan, M. A. Wildman, J. O. Ehresmann, P. W. Kletnieks and J. F. Haw, *Angew. Chem. Int. Ed.*, 2006, **45**, 3133-3136.
37. D. Lesthaeghe, V. Van Speybroeck, G. B. Marin and M. Waroquier, *Angew. Chem. Int. Ed.*, 2006, **45**, 1714-1719.
38. S. J. Kim, H.-G. Jang, J. K. Lee, H.-K. Min, S. B. Hong and G. Seo, *Chem. Commun.*, 2011, **47**, 9498-9500.
39. J. Li, Y. Wei, J. Chen, P. Tian, X. Su, S. Xu, Y. Qi, Q. Wang, Y. Zhou and Y. He, *J. Am. Chem. Soc.*, 2011, **134**, 836-839.
40. S. Svelle, P. A. Ronning and S. Kolboe, *J. Catal.*, 2004, **224**, 115-123.
41. S. Svelle, P. O. Ronning, U. Olsbye and S. Kolboe, *J. Catal.*, 2005, **234**, 385-400.
42. A. Sassi, M. A. Wildman and J. F. Haw, *J. Phys. Chem. B*, 2002, **106**, 8768-8773.
43. M. Bjorgen, S. Akyalcin, U. Olsbye, S. Benard, S. Kolboe and S. Svelle, *J. Catal.*, 2010, **275**, 170-180.
44. X. Wang, W. Dai, G. Wu, L. Li, N. Guan and M. Hunger, *Catal. Sci. Tech.*, 2014, **4**, 688-696.
45. J. Wellendorff, K. T. Lundgaard, A. Møgelhøj, V. Petzold, D. D. Landis, J. K. Nørskov, T. Bligaard and K. W. Jacobsen, *Phys. Rev. B*, 2012, **85**, 235149.
46. J. Enkovaara, C. Rostgaard, J. J. Mortensen, J. Chen, M. Duřak, L. Ferrighi, J. Gavnholt, C. Glinsvad, V. Haikola and H. Hansen, *J. Phys.: Condens. Matter*, 2010, **22**, 253202.
47. G. Kresse and D. Joubert, *Phys. Rev. B*, 1999, **59**, 1758.
48. H. J. Monkhorst and J. D. Pack, *Phys. Rev. B*, 1976, **13**, 5188-5192.
49. R. Y. Brogaard, B. M. Weckhuysen and J. K. Nørskov, *J. Catal.*, 2013, **300**, 235-241.
50. G. Henkelman, B. P. Uberuaga and H. Jónsson, *J. Chem. Phys.*, 2000, **113**, 9901-9904.
51. Y. Jeanvoine, J. G. Ángyán, G. Kresse and J. Hafner, *J. Phys. Chem. B*, 1998, **102**, 5573-5580.
52. J. P. Perdew, K. Burke and M. Ernzerhof, *Phys. Rev. Lett.*, 1996, **77**, 3865-3868.
53. M. Dion, H. Rydberg, E. Schröder, D. C. Langreth and B. I. Lundqvist, *Phys. Rev. Lett.*, 2004, **92**, 246401.

54. K. Lee, É. D. Murray, L. Kong, B. I. Lundqvist and D. C. Langreth, *Phys. Rev. B*, 2010, **82**, 081101.
55. Z. Li, J. Martínez-Triguero, P. Concepción, J. Yu and A. Corma, *Phys. Chem. Chem. Phys.*, 2013, **15**, 14670-14680.
56. S. Ilias, R. Khare, A. Malek and A. Bhan, *J. Catal.*, 2013, **303**, 135-140.

**Fig. 1** Structures of HSAPO-34 (left) and HMB/HSAPO-34 (right) using periodic 36T model.

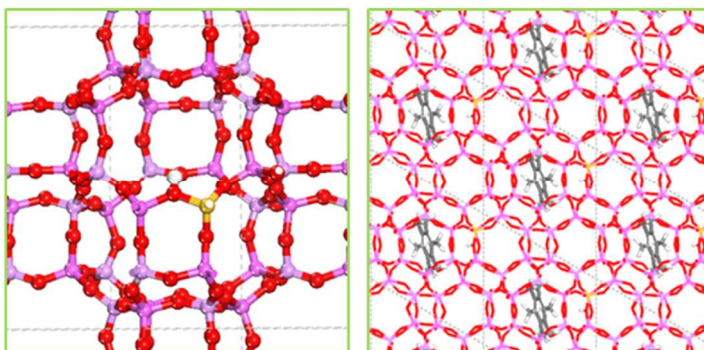


**Fig. 2** Energy diagram of HMB-based side chain HP mechanism in HSAPO-34 using BEEF-vdW (in color) and PBE (in gray) functionals. The relative energies of intermediates and transition states with respect to M0 are listed in eV.

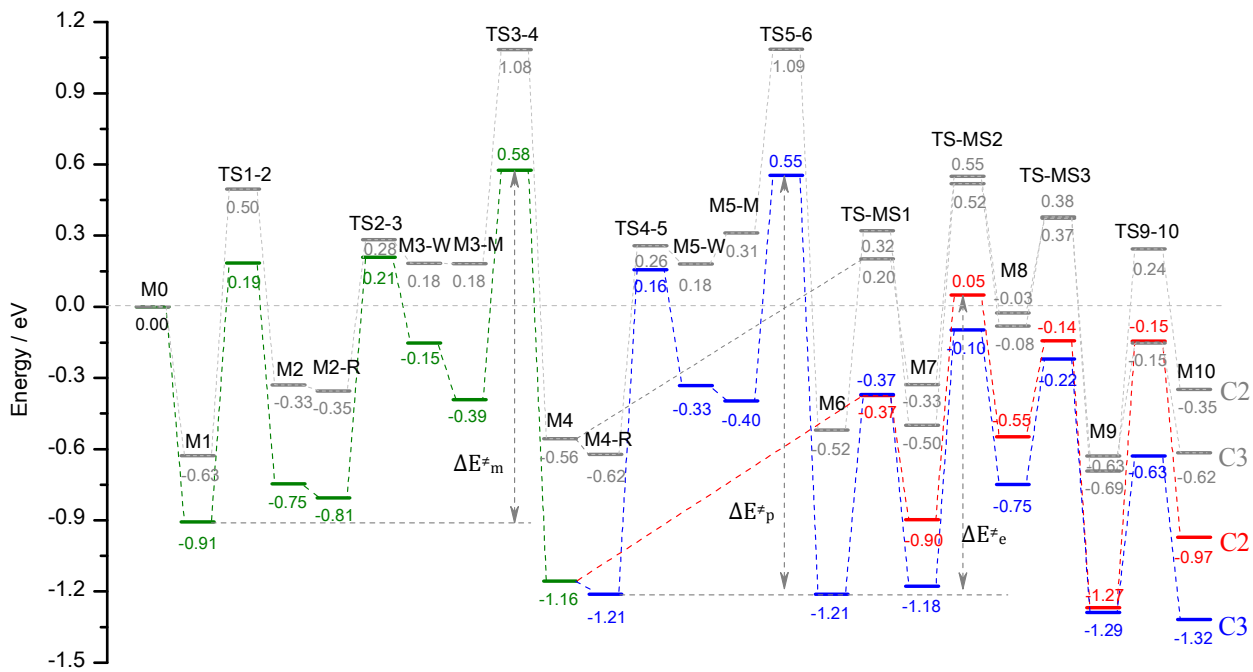


**Fig. 3** Some represented transition state structures in the methylation steps (TS1-2, TS3-4, TS5-6), methyl group shift step (TS-MS2/C2), and elimination of ethyl (TS9-10/C2) and isopropyl (TS9-10/C3) groups in HMB-based side chain HP mechanism. The bond breaking or forming distances in the transition states are in Å.

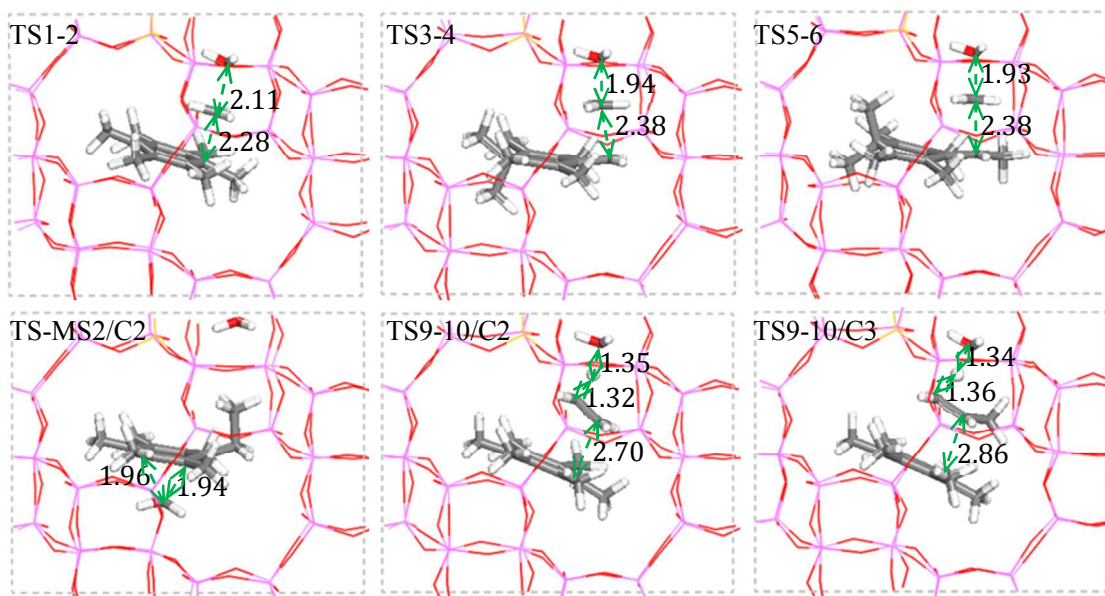


**Fig. 4** Energy diagrams of TMB-based and PX-based side chain HP mechanism in HSAPO-34 using BEEF-vdW functional. The relative energies of intermediates and transition states with respect to M0 are listed in eV.

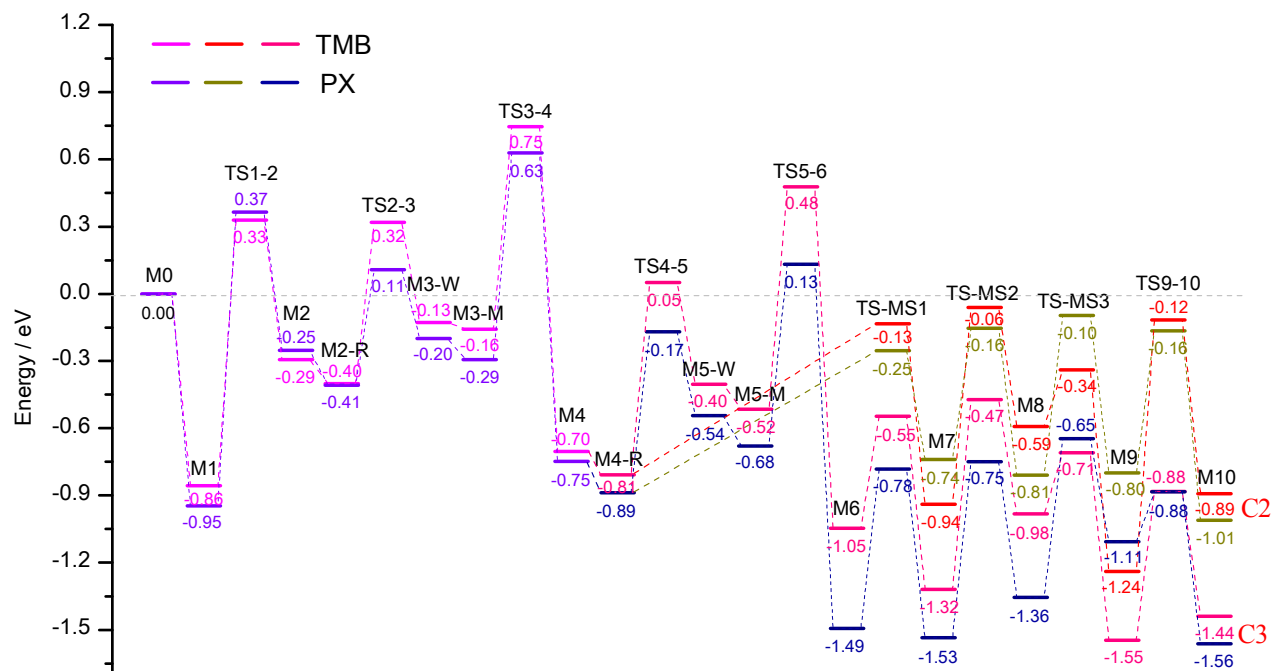


**Table 1** Energy barriers of the elementary steps in HMB-based side chain HP mechanism. All values are in eV.

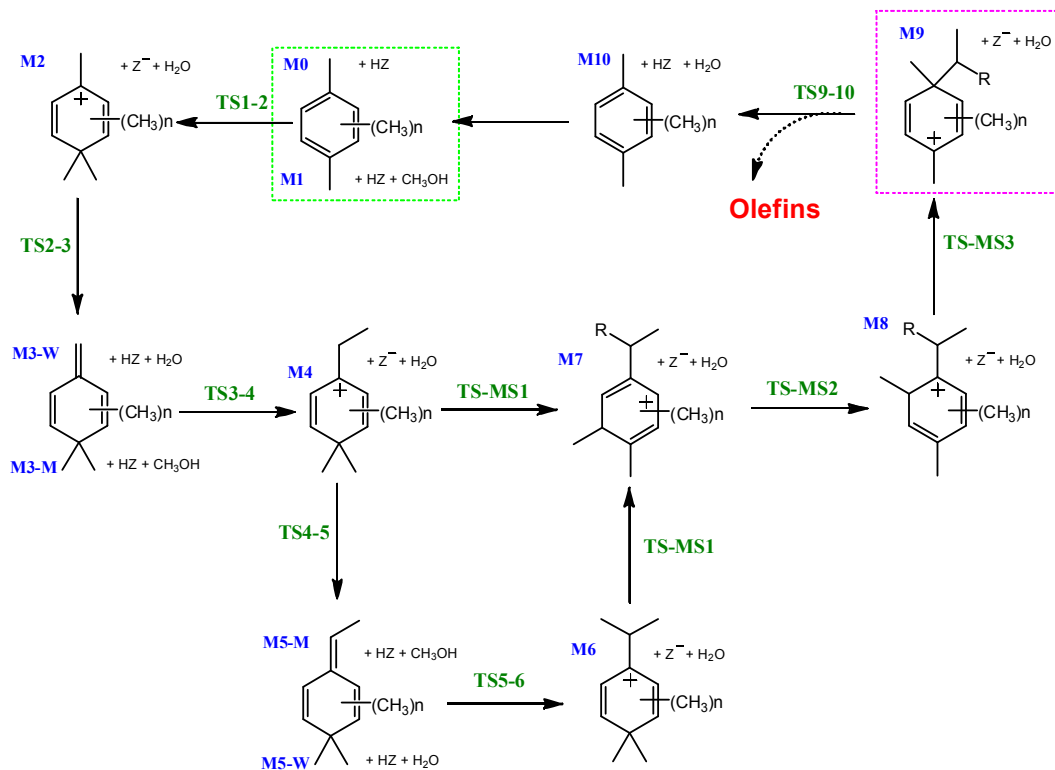
Model	36T/PBC				44T/Cluster <sup>28</sup>	12T/PBC <sup>27</sup>	
	BEEF-vdW	vdW-DF	vdW-DF2	PBE	B3LYP-D3:PM3	PBE	PBE-D
TS1-2	1.09	0.99	0.93	1.12	0.80	1.17	1.10
TS2-3	1.02	1.04	0.95	0.64	0.52	0.79	0.70
TS3-4	0.97	0.84	0.81	0.90	0.84	0.92	0.77
TS4-5	1.37	1.35	1.32	0.88	0.78	1.28	1.08
TS5-6	0.95	0.85	0.74	0.77	0.75	0.93	0.78
TS-MS1/C2	0.78	0.77	0.80	0.76	0.84		
TS-MS2/C2	0.95	0.93	0.96	0.88	0.89		
TS-MS3/C2	0.40	0.42	0.47	0.40	0.70		
TS9-10/C2	1.12	1.01	0.90	0.94	0.63		
TS-MS1/C3	0.84	0.83	0.91	0.84	0.88		
TS-MS2/C3	1.08	1.06	1.12	1.02	0.91		
TS-MS3/C3	0.53	0.50	0.61	0.46	0.90		
TS9-10/C3	0.66	0.56	0.43	0.48	0.35		

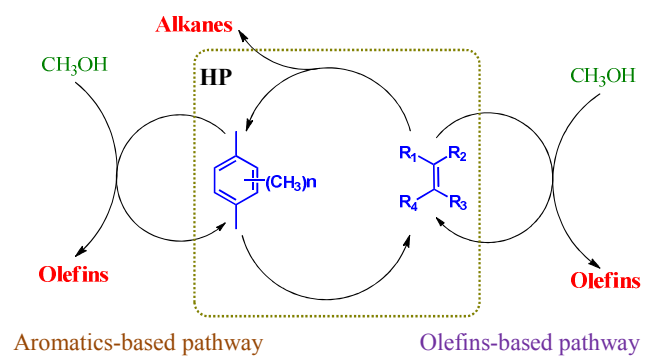
**Table 2** Energy barriers of the elementary steps in TMB-based and PX-based side chain HP mechanism. All values are in eV.

MBs	TMB						PX					
Model	36T/PBC				12T/PBC <sup>27</sup>		36T/PBC				12T/PBC <sup>27</sup>	
XC	BEEF-vdW	vdW-DF	vdW-DF2	PBE	PBE	PBE-D	BEEF-vdW	vdW-DF	vdW-DF2	PBE	PBE	PBE-D
TS1-2	1.19	1.08	1.03	1.24	1.35	1.26	1.31	1.20	1.14	1.36	1.30	1.23
TS2-3	0.61	0.63	0.60	0.27	0.46	0.45	0.52	0.57	0.54	0.10	0.48	0.46
TS3-4	0.90	0.80	0.72	0.83	0.91	0.81	0.92	0.82	0.76	0.87	0.97	0.85
TS4-5	0.86	0.88	0.86	0.42	0.50	0.43	0.72	0.80	0.79	0.30	0.56	0.43
TS5-6	0.99	0.89	0.80	0.99	0.92	0.84	0.81	0.65	0.60	0.86	1.03	0.94
TS-MS1/C2	0.57	0.58	0.61	0.50			0.49	0.50	0.51	0.47		
TS-MS2/C2	0.88	0.86	0.91	0.89			0.58	0.59	0.65	0.62		
TS-MS3/C2	0.25	0.25	0.32	0.29			0.71	0.72	0.75	0.67		
TS9-10/C2	1.12	1.05	0.97	0.94			0.64	0.57	0.46	0.47		
TS-MS1/C3	0.50	0.51	0.59	0.43			0.71	0.70	0.76	0.66		
TS-MS2/C3	0.85	0.83	0.87	0.83			0.78	0.78	0.82	0.76		
TS-MS3/C3	0.27	0.28	0.35	0.29			0.71	0.71	0.74	0.67		
TS9-10/C3	0.66	0.59	0.46	0.45			0.22	0.19	0.15	0.09		

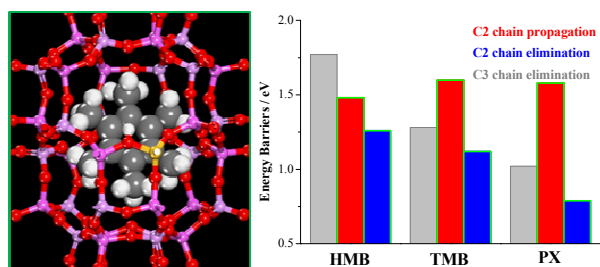
**Table 3** Overall energy barriers for the formation of side ethyl chain ( $\Delta E^\ddagger_m$ ), the production of propene ( $\Delta E^\ddagger_p$ ) and ethene ( $\Delta E^\ddagger_e$ ) through methyl group shift and elimination steps. The unit is eV.

	XC	Rate-determining States	BEEF-vdW	vdW-DF	vdW-DF2	PBE
HMB	$\Delta E^\ddagger_m$	M1 $\rightarrow$ TS3-4	1.48	1.39	1.35	1.71
	$\Delta E^\ddagger_p$	M4-R $\rightarrow$ TS5-6	1.77	1.71	1.62	1.71
	$\Delta E^\ddagger_e$	M4-R $\rightarrow$ TS-MS2	1.26	1.23	1.37	1.17
TMB	$\Delta E^\ddagger_m$	M1 $\rightarrow$ TS3-4	1.60	1.57	1.49	1.78
	$\Delta E^\ddagger_p$	M4-R $\rightarrow$ TS5-6	1.28	1.25	1.15	1.32
	$\Delta E^\ddagger_e$	M9 $\rightarrow$ TS9-10	1.12	1.05	0.97	0.94
PX	$\Delta E^\ddagger_m$	M1 $\rightarrow$ TS3-4	1.58	1.50	1.43	1.76
	$\Delta E^\ddagger_p$	M4-R $\rightarrow$ TS5-6	1.02	1.01	0.93	1.03
	$\Delta E^\ddagger_e$	M4-R $\rightarrow$ TS-MS3	0.79	0.86	0.85	0.67

**Scheme 1** MBs-based side chain hydrocarbon pool mechanism. R is H or methyl group.

**Scheme 2** Demonstration of the dual cycle mechanism proposed by Svelle et al.<sup>20-22</sup>

## Table of Contents



The dual cycle mechanism for the MTO conversion in which ethene is produced through methylbenzenes-based hydrocarbon pool cycle was verified by periodic DFT calculations with vdW correction in HSAPO-34.